Multiband conduction in the type-I clathrate Ba8Ge43 3

Christophe Candolfi, Alim Ormeci, Umut Aydemir, Michael Baitinger, Niels Oeschler, Yuri Grin, Franck Steglich

Multiband conduction in the type-I clathrate $Ba_8Ge_{43}\square_3$

C. Candolfi,* A. Ormeci, U. Aydemir, M. Baitinger, N. Oeschler, Yu. Grin, and F. Steglich
Max-Planck-Institut für Chemische Physik fester Stoffe, Nöthnitzer Straße 40, D-01187 Dresden, Germany
(Received 19 July 2011; revised manuscript received 28 September 2011; published 15 November 2011)

Hall effect and magnetoresistance measurements were carried out on a single-phase polycrystalline sample of the type-I clathrate $Ba_8Ge_{43}\square_3$ in the 2–350 K temperature range. These experiments were complemented by electronic band structure and Fermi surface calculations performed by an all-electron, full potential first-principles method. These calculations have revealed the presence of three pieces of the Fermi surface originating from both holelike and electronlike bands crossing the Fermi level suggesting that both types of carriers play a role in the electrical conduction of this material. These results were experimentally confirmed via a strongly temperature-dependent and dominant holelike signal in the Hall coefficient and a breakdown of Kohler's rule in the magnetoresistance data. We analyze the Hall coefficient and magnetoresistance data within the framework of a two-band model with temperature-dependent carrier concentrations and mobilities and discuss its limits in capturing the essential features governing the magnetotransport. Combined with the temperature dependences of the thermopower and the electrical resistivity, all these results suggest that $Ba_8Ge_{43}\square_3$ can be classified as a nearly compensated semimetal.

DOI: 10.1103/PhysRevB.84.205118 PACS number(s): 82.75.−z, 72.15.Gd

I. INTRODUCTION

Among materials exhibiting an open crystal structure in which guest atoms or molecules can be entrapped, type-I intermetallic clathrates based on a sp^3 covalently bonded framework of Si, Ge, or Sn atoms have received considerable attention due to their peculiar electrical and thermal properties.[1–5] The cubic structure of type-I clathrates contains two types of polyhedra, pentagon dodecahedra and tetrakaidecahedra, formed by the framework atoms in which alkali (Na, K, Rb, Cs), alkaline-earth (Sr, Ba), or rare-earth (Eu) metals can reside.[5,6] This host-guest nature of the crystal structure plays a key role in determining the electronic and thermal properties. In particular low thermal conductivity values are inherent to this class of compounds making them a prospective area of research to discover efficient thermoelectric materials.[1] The thermoelectric efficiency of a material is governed by the dimensionless figure of merit $ZT = \alpha^2 T/\rho\kappa$, where α is the thermopower, ρ the electrical resistivity, κ the thermal conductivity, and T the absolute temperature.[7]

A large number of investigations aimed at determining the thermoelectric potential of type-I clathrates have been undertaken.[8] Among those investigated, various compounds containing a Ge framework and Ba as guest atoms are noteworthy. High ZT values reaching 0.8 and 1.2 at ∼1000 K were discovered in the $Ba_8Ga_{16}Ge_{30}$ and $Ba_8Ni_{0.31}Zn_{0.52}Ga_{13.06}Ge_{32.2}$ compounds, respectively, demonstrating that thermoelectric properties can be significantly improved through cross substitutions of framework elements.[2,3,8]

These compounds stand for derivatives of the parent binary clathrate $Ba_8Ge_{43}\square_3$ (□ stands for a vacancy).[5] Several other phases, i.e., $Ba_8T_xGe_{46-x-y}\square_y$ (T = Al, In, Ni, Cu, Au, Pd, Pt, etc.), were synthesized, each of them exhibiting distinct crystallographic and transport properties.[9–19] The relation between the concentrations x of the substituting element and y of vacancies can usually be predicted within the Zintl rule, i.e., by assuming a complete transfer of the valence electrons of the guest atoms to the framework.[1,20] Thorough experimental and theoretical studies were then devoted to better understand the link between the variations in the vacancy concentration and the transport properties.[10–19] In addition the large phase space offered by the number of possible substitutions may help to further optimize the thermoelectric properties of $Ba_8Ge_{43}\square_3$.

However, difficulties in synthesizing single-phase samples of this parent compound prevented to unravel its intrinsic electronic properties, an essential requirement to get a deeper understanding in their evolution upon alloying. Recently, a steel-quenching technique was successfully applied to the synthesis of single-phase $Ba_8Ge_{43}\square_3$ samples, enabling a detailed characterization of both the crystal structure and transport properties.[20,21] Even though a metallic ground state in agreement with the simple electron-counting rule was revealed, measurements of transport properties showed complex temperature dependences of the thermopower and electrical resistivity. While the former exhibits two crossovers from electron to hole conduction, a transition from a low-temperature metallic state to a semiconducting-like behavior occurs near 275 K in the latter property (Fig. 1). Crystallographic studies did not show any structural transition, suggesting an electronic origin of these features. However, the exact underlying mechanism responsible for these puzzling behaviors remained an open question. Two possible mechanisms were suggested to consistently explain the temperature dependences of the electronic properties.[20] Preliminary band-structure calculations have shown that the Fermi level is positioned in a region where strong variations in the density of states (DOS) occur. A shift of the Fermi level upon increasing temperature may therefore control the observed crossovers in the thermopower via a sign change in the energy derivative of the DOS at the Fermi level. A second mechanism which may naturally explain these crossovers from n-type to p-type behavior lies in a multiband conduction involving both holes and electrons.

Here, combining first-principles calculations and Hall effect measurements up to 14 T, we show that the latter mechanism is indeed at play in $Ba_8Ge_{43}\square_3$. These calculations revealed that Fermi surfaces of both hole- and electron-type coexist in

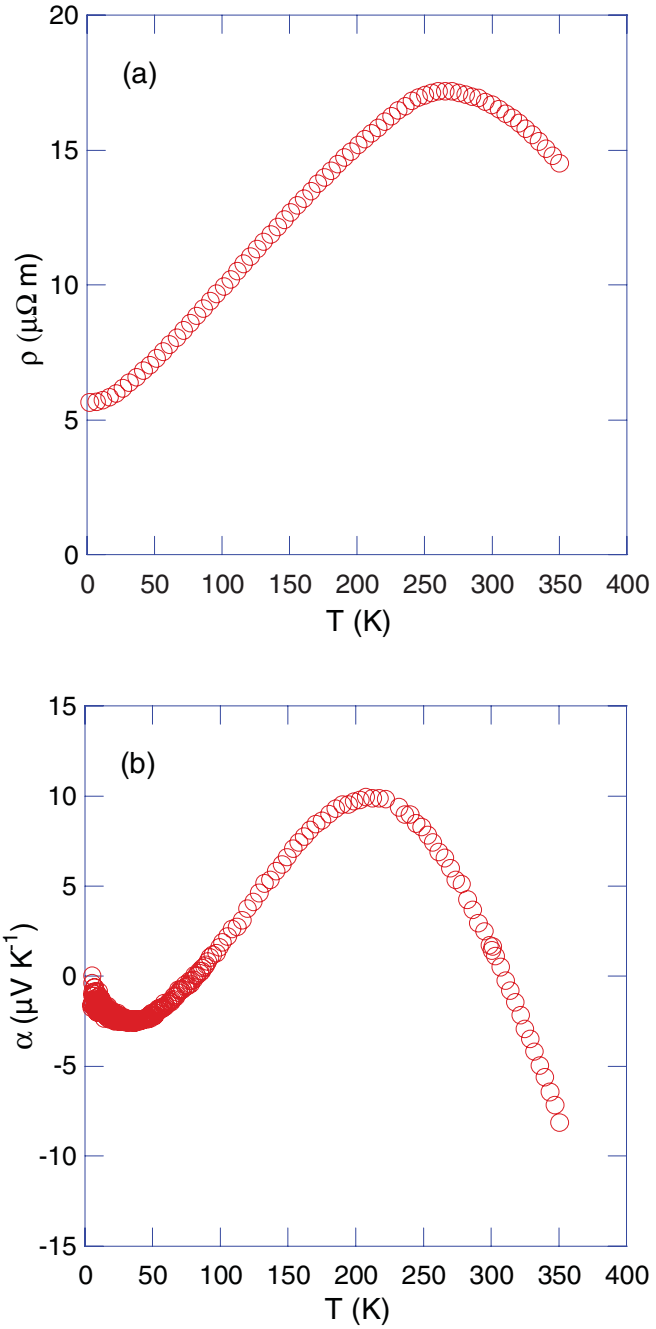

FIG. 1. (Color online) Temperature dependences of the (a) electrical resistivity and (b) thermopower of $Ba_8Ge_{43}\square_3$.

this compound. This conclusion is corroborated by the strong temperature dependence of the Hall coefficient and by the magnetoresistance data, indicating a breakdown of the Kohler's rule. Taken as a whole, our results show that $Ba_8Ge_{43}\square_3$ may be considered a nearly compensated semimetal. These results are further discussed within a two-band model and in light of prior reports on the transport properties of ternary derivatives.

II. EXPERIMENTAL AND COMPUTATIONAL DETAILS

The polycrystalline sample of $Ba_8Ge_{43}\square_3$ used in the present study was cut with a diamond-wire saw to typical dimensions $2 \times 2 \times 8$ mm^3 from the same sample batch that was previously used for transport properties measurements.[20,21] The preparation route along with a detailed description of the crystallographic and chemical characterizations was reported elsewhere.[20,21] Briefly, samples of $Ba_8Ge_{43}\square_3$ were prepared in an Ar-filled glove box. Stoichiometric mixtures of Ba (99.9%, Chempur) and Ge (99.9999%, Chempur) pieces were transferred in a glassy carbon crucible ($\varnothing = 12$ mm, $l = 12$ mm, Sigradur) and slowly heated with an induction furnace (Hüttinger, 5 kW, coil $\varnothing = 40$ mm, $l = 35$ mm; IR-pyrometer, Maurer) until a complete melt was achieved. Following that, the melt was quenched in between two polished stainless-steel plates. The phase analysis of the $Ba_8Ge_{43}\square_3$ samples was carried out by powder x-ray diffraction (PXRD), and the chemical composition was determined based on wavelength dispersive x-ray spectroscopy (WDXS) results.[20] These experiments revealed that the samples show an excellent chemical homogeneity without any detectable secondary phase. A homogeneity range could not be identified within the detection limit of PXRD and WDXS. Single crystal x-ray diffraction experiments showed that, due to the ordering of the vacancies, $Ba_8Ge_{43}\square_3$ crystallizes in the space group $Ia\bar{3}d$ with doubled unit cell parameter of $2a$ compared to the ideal type-I clathrate structure with the space group $Pm\bar{3}n$ (Fig. 2). The two different polyhedra of the type-I clathrate are preserved in the crystal structure of $Ba_8Ge_{43}\square_3$. The Ba atoms are located at the sites $16a$ and $48g$ residing in these polyhedra. The vacancies in the crystal structure of type-I clathrates are generally found at the site $6c$ in the space group $Pm\bar{3}n$. In the direct subgroup of $Ia\bar{3}d$, the $6c$ site splits to $24c$ site, refined to be almost empty (occ. $\approx 6\%$) and $24d$ site found to be almost fully occupied (occ. $\approx 94\%$).[20]

Hall effect measurements were performed with the ac transport option of a PPMS (Physical Property Measurement System, Quantum Design) from 2 up to 350 K at magnetic fields ranging between -9 and $+9$ T by a five-probe method using copper wires carefully attached onto the sample with a tiny amount of silver paste. Additional measurements up to 14 T were carried out at selected temperatures. To dismiss any longitudinal magnetoresistive contribution arising from misalignments of contacts, the Hall resistivity ρ_H was derived

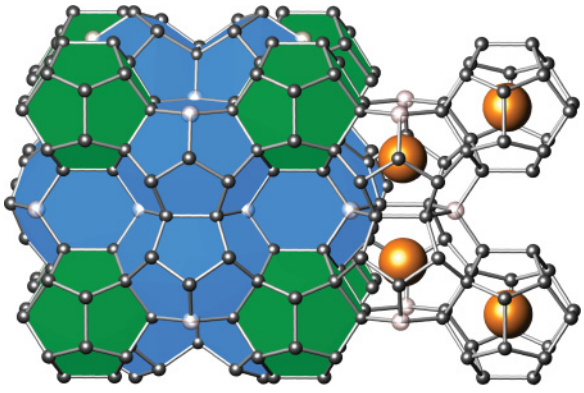

FIG. 2. (Color online) The crystal structure of the type-I clathrates. The pentagon dodecahedra and tetrakaidecahedra are shown in green and blue colors, respectively. The "guest" atoms are shown in orange and possible vacancy positions in white.

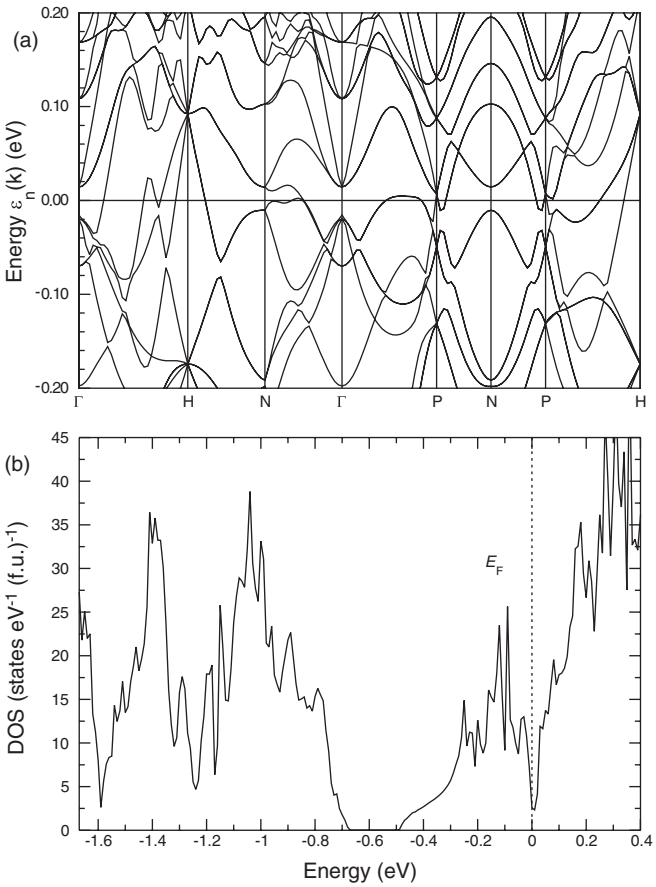

FIG. 3. (a) Electronic band structure around the Fermi level of $Ba_8Ge_{43}\square_3$ along high-symmetry directions. (b) Magnification of the energy dependence of the total DOS around the Fermi level.

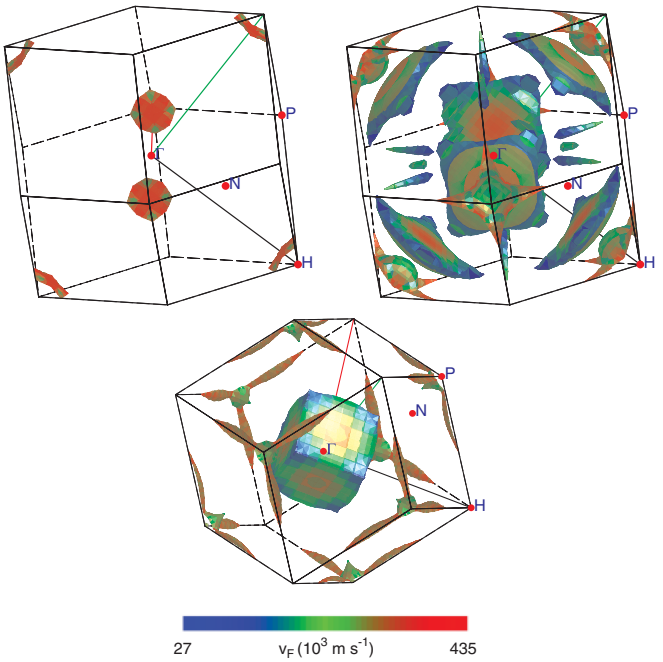

FIG. 4. (Color online) Fermi surface of the type-I clathrate $Ba_8Ge_{43}\square_3$. The upper left panel, upper right panel, and lower panel correspond to the first, second, and third band crossing the Fermi level, respectively. The shading is by Fermi velocity.

from the antisymmetric part of the transverse resistivity ρ_{xy} under magnetic field reversal following the formula $\rho_H = (\rho_{xy}(+\mu_0 H) - \rho_{xy}(-\mu_0 H))/2$.

Electronic-band structure and Fermi-surface calculations were carried out using the all-electron, full-potential local orbital method (FPLO) within the local density approximation to the density functional theory.[22] Exchange-correlation effects were accounted for through the Perdew-Wang parameterization.[23] The fully ordered $2 \times 2 \times 2$ superstructure reported in Ref. 24 with vacancies at 24*c* positions were used in our calculations. Despite the large unit cell (204 atoms in the primitive cell), we were able to employ an $8 \times 8 \times 8$ k-point grid for the Brillouin zone (BZ) integrations to accurately calculate the Fermi surface.

III. RESULTS AND DISCUSSION

The electronic structure of $Ba_8Ge_{43}\square_3$ is shown in Figs. 3(a), (b) and 4, which display the calculated band structure, the electronic DOS, and the Fermi surface, respectively. This material is metallic, as shown by the finite DOS value of 2.6 states.eV^{-1}.(f.u.)$^{-1}$ at E_F dominated by the contribution of Ge atoms. Interestingly, this value seems to decrease as more accurate electronic structure calculation method and denser sampling of the BZ are used. A linear muffin-tin orbital approach within the atomic sphere approximation found 9.9 states.eV^{-1}.(f.u.)$^{-1}$ with 216 k-points in full BZ, while the FPLO method with the same sampling gives a lower value of 2.9 states.eV^{-1}.(f.u.)$^{-1}$. Pseudopotential and full-potential linearized augmented plane-wave method calculations carried out in a simple cubic model structure (note that the reported superstructure with fully ordered vacancies was not used and no information on the BZ sampling was provided) gave a considerably larger value of 20 states.eV^{-1}.(f.u.)$^{-1}$ (see Ref. 20 and references therein). The Fermi level lies near a deep local minimum, which can be regarded as a pseudo-gap (Fig. 3) and may explain the sensitivity of the calculated DOS value to the method and the BZ sampling utilized.

Three bands of both electron- and hole-type character cross the Fermi level. The first band around the H point gives rise to a portion of the Fermi surface consisting of platelike surfaces at the zone corner associated to hole-type carriers exhibiting a high Fermi velocity (Fig. 4). This surface gives a small contribution to the DOS at the Fermi level $N(E_F)$, which only amounts to 0.08 states.eV^{-1}.(f.u.)$^{-1}$. The second band is more complex and is predominantly composed of hole-type bands with a small admixture of an electron-type band. The former are located around the H point between Γ and H (with the shape of an umbrella) and between Γ and P, while the latter is visible between Γ and N. The corresponding Fermi-surface portion is composed of four three-dimensional and disconnected surfaces around the Γ point, the small pockets of slow-moving electrons consisting of rod-shaped surfaces. Those pieces of the Fermi surface due to the third band also contain charge carriers of both signs. Of the two electron-type surfaces, one is a very large cubelike surface centered at the Γ point. The other one is centered around the P point and extends toward

H in a rodlike fashion. The hole-type surface is extremely tiny and centered around the P point (it appears in Fig. 4 as a very small green point at P). The presence of both electron- and hole-type surfaces suggests that $Ba_8Ge_{43}\square_3$ features a multiband conduction from which the complex temperature dependence of the thermopower emerges (Fig. 1).[20,21] Further, the total areas of the hole- and electron-type surfaces seem to be qualitatively similar hinting at a possible nearly compensated nature of this compound.

A conclusive experimental evidence for the multiband nature of the electrical conduction in $Ba_8Ge_{43}\square_3$ is provided by the magnetic field dependence of the Hall resistivity ρ_H, shown in Figs. 5(a) and 5(b) at selected temperatures. In the whole temperature and magnetic field ranges covered, ρ_H evolves linearly with H, the positive slope reflecting the dominance of holes which contrasts with the thermopower data revealing temperature windows where an n-type conduction prevails (Fig. 1).[20,21] These results therefore clearly indicate contributions from both hole- and electronlike orbits on the Fermi surface, as suggested by our band-structure calculations. The $\rho_H(\mu_0 H)$ data retain a linear dependence regardless of temperatures indicating that, up to 14 T, electrons remain in the low-field limit $\omega_c\tau \ll 1$ where $\omega_c = e\mu_0 H/m^*$ is the cyclotron frequency and τ is the scattering time. From the slope of the isothermal $\rho_H(\mu_0 H)$ curves, the temperature dependence of the Hall coefficient $R_H = \rho_H/\mu_0 H$ can be inferred. As shown in Fig. 6, R_H displays a strong temperature dependence in sharp contrast to a T-independent behavior expected in simple metals. The R_H values first decrease from 1.40×10^{-2} down to 0.10×10^{-2} $cm^3.C^{-1}$ near ~280 K before increasing above this temperature up to 350 K to reach 1.55×10^{-2} $cm^3.C^{-1}$.

Within a single-band picture R_H is related to the hole concentration n_h via the relation $n_h = 1/R_h e$ where e is the elementary charge. In the present case this relation gives an upper limit of the hole concentration and yields a variation in n_h from 4.5×10^{20} cm^{-3} at 10 K to 3.4×10^{21} cm^{-3} at 300 K. Such a low-carrier density correlates with the high electrical resistivity values and implies portion of the Fermi surface occupying a small part of the BZ.

The magnetoresistance $\Delta\rho_{xx}(\mu_0 H,T)/\rho_{xx}(0,T) = [\rho_{xx}(\mu_0 H,T) - \rho_{xx}(0,T)]/\rho_{xx}(0,T)$, where $\rho_{xx}(\mu_0 H,T)$ and $\rho_{xx}(0,T)$ are the longitudinal resistivity at a magnetic field $\mu_0 H$ and that at zero magnetic field, respectively, provides another probe of the multiband conduction in $Ba_8Ge_{43}\square_3$. The magnetoresistance data, collected up to 14 T and shown in Fig. 7(a) at selected temperatures, are positive over the whole temperature range and originate from the bending of the charge carrier trajectory by the Lorentz force. In simple metals the magnetoresistance displays quadratic field dependence at low fields and saturates at high fields.[25] As shown in Fig. 7(a), while the magnetoresistance demonstrates the former dependence, no sign of saturating behavior up to 14 T is observed. This behavior, combined with a low carrier density, suggests that $Ba_8Ge_{43}\square_3$ is a nearly compensated semimetal. In such a case a sizeable magnetoresistance can emerge as compared to the low values usually encountered in simple and uncompensated metals.[25] This appears in agreement with the temperature dependence of the magnetoresistance shown in Fig. 7(b). The magnetoresistance amounts to ~5% at 10 K,

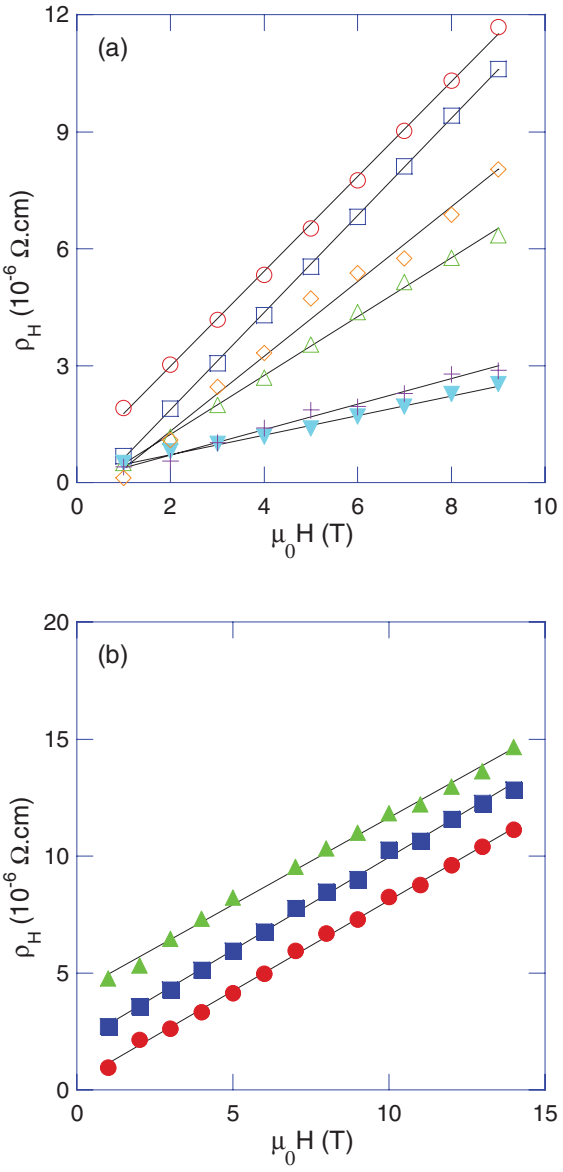

FIG. 5. (Color online) (a) Hall resistivity ρ_H as a function of the applied magnetic field $\mu_0 H$ at T = 10 (open red circle), 60 (open blue square), 155 (open green triangle), 210 (blue-filled inverted triangle), 310 (purple plus), and 340 K (open orange diamond). (b) ρ_H as a function of the magnetic field measured up to $\mu_0 H = 14$ T at T = 10 (blue-filled square), 5 (green-filled triangle), and 2 K (red-filled circle). In both panels the solid lines stand for the best fit to the data highlighting the linear behavior of $\rho_H(\mu_0 H)$ in the whole temperature range and up to $\mu_0 H = 14$ T. Note that for sake of clarity, a vertical offset have been applied to some of the data presented.

decreases with increasing temperature up to ~250 K, before increasing again to reach ~2.2% at 350 K. Interestingly, the minimum observed in the magnetoresistance is concomitant to that observed in the R_H data and to the maximum in the electrical resistivity, suggesting a common electronic origin of these features.

An alternative way to unravel the contribution of both carriers from the magnetoresistance data is related to the so-called Kohler's plot. In a single-band system with isotropic

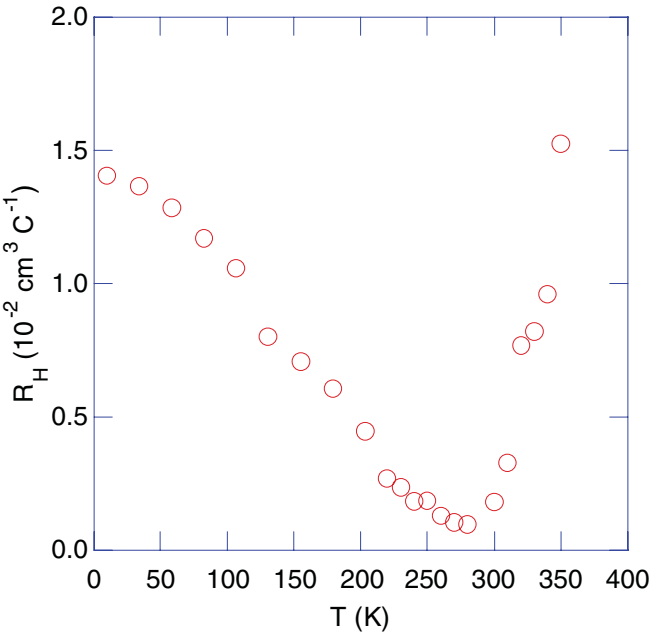

FIG. 6. (Color online) Temperature dependence of the Hall coefficient R_H.

relaxation times at all points on the Fermi surface, the magnetoresistance is expected to follow the Kohler's rule expressed as[25]

$$\frac{\Delta\rho_{xx}}{\rho_{xx}} = f\left(\frac{\mu_0 H}{\rho_{xx}}\right), \tag{1}$$

where $f(x)$ is a temperature-independent implicit function. This relation implies that the $\Delta\rho_{xx}/\rho_{xx}$ versus $\mu_0 H/\rho_{xx}$ curves taken at different temperatures should merge into a single universal curve. However, in a system featuring multiband effects a deviation from this scaling law is expected to occur, as is indeed observed in the present case (Fig. 8).

Both Hall effect and magnetoresistance data have demonstrated that holes and electrons contribute to the electrical conduction in this material. This property is therefore at the origin of the temperature dependence of the thermopower and electrical resistivity shown in Fig. 1. In a multiband system the thermopower can be expressed as

$$\alpha = \frac{\sum_i \sigma_i \alpha_i}{\sum_i \sigma_i}, \tag{2}$$

where σ_i is the partial electrical conductivity of the ith band and α_i the corresponding partial contribution to the thermopower, the sum being taken over all the bands contributing at the Fermi level. In the simple case of an electronlike and holelike two-band system, this expression reduces to

$$\alpha = \frac{\sigma_h \alpha_h + \sigma_e \alpha_e}{\sigma_h + \sigma_e}, \tag{3}$$

where the indices h and e refer to the hole and electron contributions, respectively. Thus, in multiband systems, $\alpha(T)$ may exhibit complex temperature dependence with possible changes in the sign as a function of the temperature. In addition a near compensation of the hole and electron contributions to the electrical and thermal conduction processes is consistent with the relatively small magnitude of α up to 350 K ($|\alpha| < 10\ \mu$V.K^{-1}, see Fig. 1). The downturn observed in $\rho(T)$ may be also explained within this scenario either by an increase in the overall carrier concentration and/or by an increase in the mobility of the charge carriers.

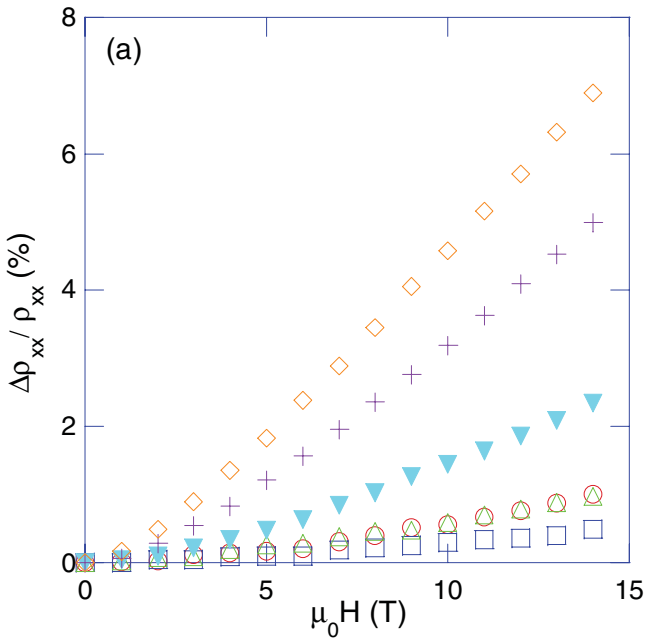

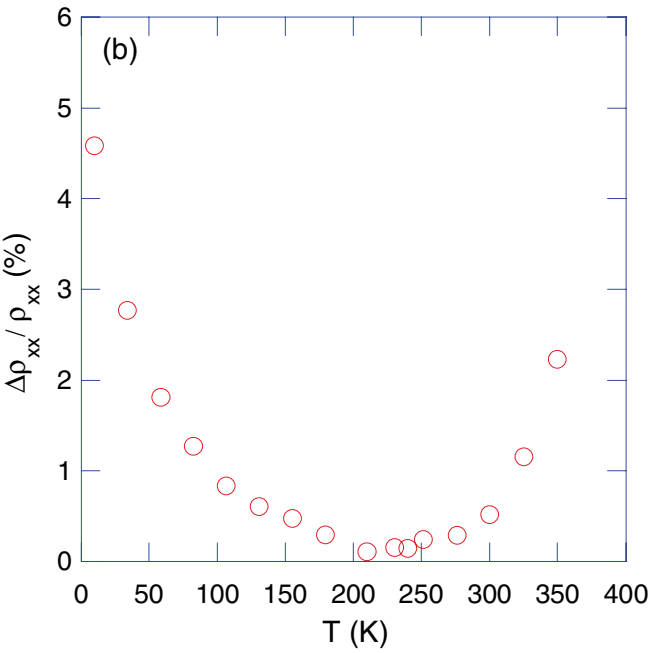

FIG. 7. (Color online) (a) Magnetic field dependence of the longitudinal electrical resistivity ρ_{xx} plotted as $\Delta\rho_{xx}/\rho_{xx}$ versus $\mu_0 H$ at T = 300 (open red circle), 250 (open blue square), 155 (open green triangle), 80 (blue-filled inverted triangle), 35 (purple plus), and 10 K (open orange diamond). (b) Temperature dependence of the magnetoresistance measured at $\mu_0 H = 9$ T.

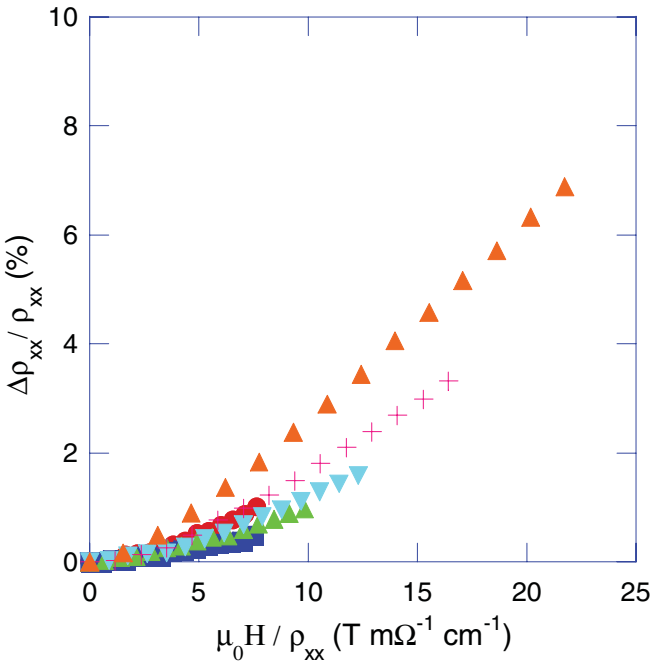

FIG. 8. (Color online) Scaled dependences of the magnetoresistance data collected at T = 300 (red-filled circle), 250 (blue-filled square), 155 (green-filled triangle), 105 (blue-filled inverted triangle), 60 (purple plus), and 10 K (orange-filled triangle) plotted as a function of $\mu_0 H/\rho_{xx}$ revealing a clear departure from the Kohler's rule.

Even though our calculations have revealed that the Fermi level intersects three bands giving rise to a complex Fermi surface, the simultaneous presence of holes and electrons raises the question as to which extent a two-band model can account for the observed data. To verify whether this description may capture the essential physics involved in the magnetotransport in this material, we analyzed the magnetoresistance and the Hall data within a two-band model with temperature-dependent mobilities and concentrations of holes and electrons. The magnetoresistance, along with the temperature dependence of the thermopower, have yielded hints suggesting a nearly compensated semimetallic state in this material. This could in principle lead to a simplification of the two-band model by assuming an equal concentration of holes and electrons. However, we started from a general model of an uncompensated two-band metal. As shown subsequently, this model further suggests a nearly compensated ground state in $Ba_8Ge_{43}\square_3$. Within this framework the magnetoresistance, in the low-field limit, can be expressed as[25]

$$\Delta\rho_{xx}(H,T)/\rho_{xx}(0,T) = MR_\infty(T)\frac{\mu^2H^2}{1+\mu^2H^2}, \tag{4}$$

where

$$MR_\infty = \frac{R_h\sigma_h + R_e\sigma_e}{\sigma_h\sigma_e(R_h - R_e)^2} \tag{5}$$

and

$$\mu = \left|\frac{\sigma_h\sigma_e(R_h - R_e)}{\sigma_h + \sigma_e}\right|. \tag{6}$$

In these relations μ stands for the effective mobility, R_h and R_e are the respective Hall coefficients of the hole and electron contributions, and σ_h and σ_e are the partial hole and electron conductivities, respectively. The electrical conductivity and the Hall coefficient are expressed as

$$\sigma = \sigma_e + \sigma_h \tag{7}$$

and

$$R_H(H,T) = \frac{R_{H0}(T) + R_{H\infty}(T)\mu^2H^2}{1+\mu^2H^2}, \tag{8}$$

where

$$R_{H0} = \frac{\sigma_h^2R_h - \sigma_e^2R_e}{(\sigma_h+\sigma_e)^2} \tag{9}$$

and

$$R_{H\infty} = \frac{-R_hR_e}{R_h - R_e}. \tag{10}$$

A fit of the magnetoresistance data at each temperature yields the values of the μ and MR_∞ parameters. Then, simultaneously solving Eqs. (5), (6), (7), and (8), the Hall coefficients R_h and R_e, along with the partial conductivities σ_h and σ_e, provide the temperature dependences of the concentrations and mobilities of holes and electrons via the relations $n_{(h,e)} = 1/e|R_{(h,e)}|$ and $\mu_{(h,e)} = |R_{(h,e)}|\sigma_{(h,e)}$.

The temperature dependences of n_h and n_e are depicted in Fig. 9(a). The hole and electron-carrier concentrations inferred are of the same order of magnitude (10^{18} cm^{-3}), n_h being slightly higher than n_e in the whole temperature range. The low-carrier densities and the almost equal concentrations of holes and electrons further support the idea that $Ba_8Ge_{43}\square_3$ possesses a nearly compensated semimetallic ground state. With decreasing temperature the mobilities of both types of carriers show an overall increase from ~500 cm^2.V^{-1}.s^{-1} at 250 K to ~1100 cm^2.V^{-1}.s^{-1} at 10 K [Fig. 9(b)]. Above ~250 K, the mobility of holes and electrons tends to increase with increasing temperature, which may be the reason for the downturn observed in the electrical resistivity data.

The previously mentioned values of the mobility should imply a violation of the low-field approximation ($\omega_c\tau \approx 1$) at a characteristic field of $\mu_0 H \sim 20$ T at 300 K decreasing to 10 T at 10 K. This last field value should in principle lead to a deviation from linearity in the $\rho_H(\mu_0 H)$ data measured below 10 K while clearly no such curvature shows up in our experimental data at least up to 14 T [see Fig. 5)]. This contradiction may therefore reflect the limits of this model, which tends to overestimate the mobilities of the charge carriers. The absence of nonlinear behavior up to 14 T gives an upper limit of the electron mobility of ~750 cm^2.V^{-1}.s^{-1} at 2 K. However, whether this overestimation only exists at low temperatures or extends up to room temperature is still an open question. Nevertheless, this model predicts a compensated state with low densities of holes and electrons, which is consistent with the temperature dependences of the thermopower, electrical resistivity, and with our first-principles calculations. Further measurements performed at higher magnetic fields would be illuminating in determining the characteristic field, if any, at which electrons give rise to a nonlinear behavior in the $\rho_H(\mu_0 H)$ curves and would help

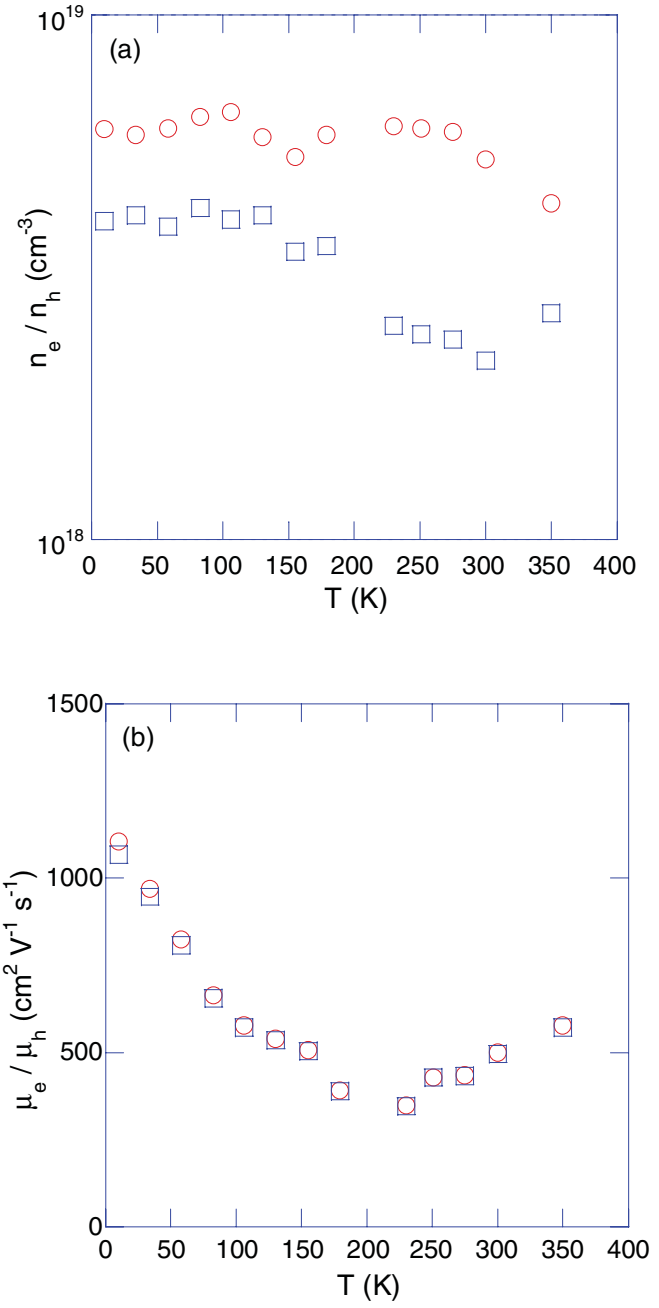

FIG. 9. (Color online) Temperature dependence of the hole (open red circle) and electron (open blue square) concentrations (a) and mobilities (b) derived from a two-band model.

clarify whether or not a description within a two-band model is pertinent in the present case.

The peculiar transport properties of $Ba_8Ge_{43}\square_3$ raise another intriguing question as for the evolution of the nearly compensated state upon alloying and when the ordered vacancy sublattice is destroyed. This last situation can be realized via a partial substitution on the Ge sites. It is therefore instructive to consider the ternary systems investigated so far with a particular emphasis on low substitution levels for which the main features of the band structure of $Ba_8Ge_{43}\square_3$ may be preserved. In this regard investigations on the clathrates $Ba_8M_xGe_{46-x-y}\square_y$ for M = Zn, Pd, Pt, and Cd have revealed that at low x values, the temperature dependence of the electrical resistivity is similar to that of the binary compound, i.e., a metallic behavior prevails at low temperatures followed by a downturn mimicking a semiconducting-like dependence.[9–12] However, the magnitude of $\rho(T)$ and the temperature at which the maximum in $\rho(T)$ occurs are influenced by both the nature of the element and its concentration. For instance, in the $Ba_8Cd_xGe_{46-x-y}\square_y$ compounds at $x = 2.4$, the maximum is shifted to ~225 K compared to the parent compound.[9] Increasing the Cd content to $x = 4.7$ leads to a further shift of this maximum to ~190 K together with a more pronounced variation in the $\rho(T)$ values. In the Zn, Pd, and Pt systems, a similar behavior was observed at $x = 2.1$, 2.0, and 2.0, respectively.[10–12] Since none of these compounds exhibits a superstructure, these results suggest that the ordered vacancy sublattice plays a secondary role in determining the electrical properties in these compounds.

In these prior studies the presence of this maximum has been attributed to a gapped DOS near E_F giving rise to an activated behavior reflecting the thermal excitation of the carriers across the band gap. However, in light of the present results, a rather different picture emerges. The observed behavior may be related to the simultaneous presence of hole and electron Fermi surfaces, a conclusion which seems further corroborated by recent electronic band structure calculations performed on $Ba_8Cd_xGe_{46-x-y}\square_y$.[26] These calculations have shown that, regardless of the Cd content, the band structure does not exhibit a band gap near E_F. The number of bands intersected by the Fermi level evolves from two bands for $x = 2$ to three bands for Cd contents up to $x = 8$. At low Cd concentrations ($x = 2$ and $x = 4$), the conduction and valence bands overlap classifying these compounds as semimetals while the $x = 6$ and $x = 8$ samples are metallic in nature. These results are in excellent agreement with the experimental $\rho(T)$ data reported by Melnychenko-Koblyuk *et al.*[9] and with our data collected on $Ba_8Ge_{43}\square_3$. Hall measurements which would provide decisive clues were however not reported for these ternary compounds and should therefore be the focus of future studies.

Thermopower measurements performed on these systems indicate a stronger sensitivity of this property to the composition with respect to the electrical resistivity. The features observed in the thermopower data of $Ba_8Ge_{43}\square_3$ are suppressed in the Cd, Pd, and Pt systems.[9,11,12] The Zn system, however, shows a more complex behavior.[10] At $x = 2.1$, $\alpha(T)$ exhibits a nonlinear temperature dependence though the measured values remain negative in the whole temperature range. A further increase of the Zn content ($x = 4.7$) then modifies the low temperature behavior, which is recovered at $x = 6.1$. At this concentration, slightly positive values ($<0.5\mu V.K^{-1}$) can be observed around ~75 K. These nonmonotonic variations reflect the strong modifications of the electronic band structure against the Zn content, which cannot be accounted for by a simple rigid-band model.[27] Clearly, all these studies highlight the sensitivity of the electronic band structure to the concentration and the nature of the substituting element and also show that a multiband conduction may be preserved over a rather large concentration window in ternary systems.

IV. CONCLUSION

Detailed measurements of the Hall coefficient and magnetoresistance in the type-I clathrate $Ba_8Ge_{43}\square_3$ have demonstrated the influential role played by holes and electrons in the electrical transport properties. This conclusion is further corroborated by first-principles calculations of the electronic band structure and Fermi surface taking explicitly into account the ordered vacancy sublattice. All these results suggest that $Ba_8Ge_{43}\square_3$ is a nearly compensated semimetal. Though a two-band model predicts similar electron and hole concentrations, this approximation leads to overestimated charge carrier mobilities, suggesting that this model may not be fully adequate in the present case. A survey of prior results obtained in ternary systems $Ba_8M_xGe_{46-x-y}\square_y$ has shown that similar properties are preserved at low x values even in the absence of a superstructure. Our results underline a more complex picture of the evolution of the transport properties of ternary systems based on $Ba_8Ge_{43}\square_3$ upon substituting than previously thought and provide a useful reference to better understand the electronic properties of Ge-based type-I clathrates with transition metals. Future studies on ternary compounds would benefit from Hall data combined with electronic band structure calculations to determine the variations in the hole and electron contributions to the transport properties at low substitution levels.

ACKNOWLEDGMENTS

C.C. acknowledges the financial support of the CNRS-MPG program. M.B. and Yu.G. gratefully acknowledge financial support by the Deutsche Forschungsgemeinschaft (SPP 1415, "Kristalline Nichtgleichgewichtsphasen (KNG)—Präparation, Charakterisierung und *in situ*-Untersuchung der Bildungsmechanismen").

*christophe.candolfi@cpfs.mpg.de

[1] G. S. Nolas, G. A. Slack, and S. B. Schujman, in *Semiconductors and Semimetals*, edited by T. M. Tritt, Vol. 69 (Academic Press, San Diego, CA, 2011), p. 255.
[2] E. S. Toberer, M. Christensen, B. B. Iversen, and G. J. Snyder, Phys. Rev. B **77**, 075203 (2008).
[3] J. Martin, H. Wang, and G. S. Nolas, Appl. Phys. Lett. **92**, 222110 (2008).
[4] J. L. Cohn, G. S. Nolas, V. Fessatidis, T. H. Metcalf, and G. A. Slack, Phys. Rev. Lett. **82**, 779 (1999).
[5] M. Christensen, S. Johnsen, and B. B. Iversen, Dalton Trans. **39**, 978 (2010).
[6] K. A. Kovnir and A. V. Shevelkov, Russ. Chem. Rev. **73**, 923 (2004).
[7] H. J. Goldsmid, in *Thermoelectric Refrigeration*, (Temple Press Books Ltd, London, 1964), p. 43.
[8] X. Shi, J. Yang, S. Bai, J. Yang, H. Wang, M. Chi, J. R. Salvador, W. Zhang, L. Chen, and W. Wong-Ng, Adv. Funct. Mater **20**, 755 (2010).
[9] N. Melnychenko-Koblyuk, A. Grytsiv, St. Berger, H. Kaldarar, H. Michor, F. Röhrbacher, E. Royanian, E. Bauer, P. Rogl, H. Schmid, and G. Giester, J. Phys. Condens. Matter **19**, 046203 (2007).
[10] N. Melnychenko-Koblyuk, A. Grytsiv, L. Fornasari, H. Kaldarar, H. Michor, F. Röhrbacher, M. M. Koza, E. Royanian, E. Bauer, P. Rogl, M. Rotter, H. Schmid, F. Marabelli, A. Devishvili, M. Doerr, and G. Giester, J. Phys.: Condens. Matter **19**, 216223 (2007).
[11] N. Melnychenko-Koblyuk, A. Grytsiv, P. Rogl, M. Rotter, E. Bauer, G. Durand, H. Kaldarar, R. Lackner, H. Michor, E. Royanian, M. M. Koza, and G. Giester, Phys. Rev. B **76**, 144118 (2007).
[12] N. Melnychenko-Koblyuk, A. Grytsiv, P. Rogl, M. Rotter, R. Lackner, E. Bauer, L. Fornasari, F. Marabelli, and G. Giester, Phys. Rev. B **76**, 195124 (2007).
[13] S. Johnsen, A. Bentien, G. K. H. Madsen, B. B. Iversen, and M. Nygren, Chem. Mater **18**, 4633 (2006).
[14] H. Anno, M. Hokazono, M. Kawamura, J. Nagao, and K. Matsubara, in *Proceedings of the 21st International Conference on Thermoelectrics*, (IEEE, New York, 2002), pp. 77–80.
[15] A. Bentien, M. Christensen, J. D. Bryan, A. Sanchez, S. Paschen, F. Steglich, G. D. Stucky, and B. B. Iversen, Phys. Rev. B **69**, 045107 (2004).
[16] N. Nasir, A. Grytsiv, N. Melnychenko-Koblyuk, P. Rogl, I. Bednar, and E. Bauer, J. Solid State Chem. **183**, 2329 (2010).
[17] S. Y. Rodriguez, L. Saribaev, and J. H. Ross Jr., Phys. Rev. B **82**, 064111 (2010).
[18] L. T. K. Nguyen, U. Aydemir, M. Baitinger, E. Bauer, H. Borrmann, U. Burkhardt, J. Custers, A. Haghighirad, R. Höfler, K. D. Luther, F. Ritter, W. Assmus, Yu. Grin, and S. Paschen, Dalton Trans. **39**, 1071 (2010).
[19] H. Zhang, H. Borrmann, N. Oeschler, C. Candolfi, W. Schnelle, M. Schmidt, U. Burkhardt, M. Baitinger, J.-T. Zhao, and Yu. Grin, Inorg. Chem. **50**, 1250 (2011).
[20] U. Aydemir, C. Candolfi, H. Borrmann, M. Baitinger, A. Ormeci, W. Carrillo-Cabrera, C. Chubilleau, B. Lenoir, A. Dauscher, N. Oeschler, F. Steglich, and Yu. Grin, Dalton Trans. **39**, 1078 (2010).
[21] C. Candolfi, U. Aydemir, M. Baitinger, N. Oeschler, F. Steglich, and Yu. Grin, J. Electron. Mater. **39**, 2039 (2010).
[22] K. Koepernik and H. Eschrig, Phys. Rev. B **59**, 1743 (1999).
[23] J. P. Perdew and Y. Wang, Phys. Rev. B **45**, 13244 (1992).
[24] W. Carrillo-Cabrera, S. Budnyk, Y. Prots, and Yu. Grin, Z. Anorg. Allg. Chem. **630**, 2267 (2004).
[25] A. B. Pippard, *Magnetoresistance in Metals*, (Cambridge University Press, Cambridge, 1988) pp. 23, 28–30.
[26] N. A. Borshch, N. S. Pereslavtseva, and S. I. Kurganskii, Semiconductors **44**, 987 (2010).
[27] N. A. Borshch, N. S. Pereslavtseva, and S. I. Kurganskii, Semiconductors **43**, 563 (2009).